

Anomalous impurity ion heating from Alfvénic cascade in the reversed field pinch

Varun Tangri, P. W. Terry, and Gennady Fiksel

Center for Magnetic Self-Organization in Laboratory and Astrophysical Plasmas and Department of Physics, University of Wisconsin-Madison, 1150 University Avenue, Madison, Wisconsin 53706, USA

(Received 15 January 2008; accepted 19 September 2008; published online 3 November 2008)

Anomalous ion and impurity heating in reversed field pinch plasmas is addressed. Previous work [N. Mattor *et al.*, *Comments Plasma Phys. Controlled Fusion* **15**, 65 (1992)], which calculated the heating of bulk ions by gyro and Landau resonances with turbulent fluctuations cascading from unstable tearing modes, is extended to impurity species measured in Madison symmetric torus (MST). The heavier mass of impurities allows gyro-resonant heating at lower frequencies where more energy is present in the fluctuations. A 0D transport model is used to examine heating rates under various time-dependent, experimental heating scenarios, such as a sawtooth crash. Impurity heating rates calculated for impurities found in MST are comparable to observed rates inferred in the impurity temperature rise during sawtooth events. © 2008 American Institute of Physics.

[DOI: 10.1063/1.2998829]

I. INTRODUCTION

In reversed-field pinch (RFP) plasmas, strong ion heating with $T_i \geq T_e$ is frequently observed in standard Ohmic discharges.^{1–4} This observation contradicts the simple notion that in an Ohmically heated plasma, energy is predominantly dissipated by the current into electron heat as characterized by Spitzer resistivity and Ohm's law. Ions are then heated by frictional drag (through collisions with electrons). Assuming finite heat losses, this process will always result in $T_i \leq T_e$. The unknown physical process raising T_i above a value consistent with collisional transfer from Ohmically heated electrons is usually referred to as anomalous ion heating. Anomalous ion heating has been observed in several experiments, and is well documented. For example, in ZETA (Ref. 2) and present-day machines,^{1,3,4} ion energies have been observed to exceed estimates from Ohmic heating and collisional transfer from electrons. In the Caltech Encore device,⁵ anomalously fast ($\sim 40\times$ classical Ohmic) ion heating was observed. Similarly, during a sawtooth crash in the Madison symmetric torus (MST) RFP,¹ the ion temperature can spontaneously increase by several hundred eV in about 100 μ s. The corresponding change in ion thermal energy is approximately $dT_i/dt \sim 3 \times 10^6$ eV/s. During this period, the electron temperature deteriorates, possibly due to enhanced anomalous electron heat losses. This evidence points to a collisionless ion heating mechanism that is quite separate from electron thermal processes.

Anomalous ion heating is not understood despite extensive work on the subject. Numerous mechanisms have been proposed, including, frictional drag, ion Landau damping of Alfvén waves, electron cyclotron resonant (ECR) damping of Alfvén waves, viscous damping,⁶ stochastic heating,^{5,7} ion cyclotron damping of Alfvén waves,⁸ heating from slow wave continua,⁹ heating by emission from electron clumps,¹⁰ and reconnection. None of these mechanisms has been confirmed experimentally in a convincing way, and many have difficulty explaining aspects of observations.

Frictional drag, for example, leads to a very low value of the heating rate. Quantitatively, the change in thermal energy due to frictional drag is $\kappa dT_i/dt \sim e^2 E^2 \tau_{ei}/m_i \sim 150\text{--}300$ eV/s (τ_{ei} is the electron-ion collision time and κ is the Boltzmann constant). This is several orders of magnitude lower than the observed heating rate. If particles are resonant, ion Landau damping or ECR damping can be an efficient heating mechanism. However, in the RFP, ECR damping is ineffective since typical frequencies are too low ($\omega \ll \Omega_e$), yielding heating rates that are several orders of magnitude lower than observations. In a similar vein, Landau damping has been widely regarded as ineffective except at high frequencies, because phase velocities are too low ($\omega/k \ll V_{ti}$). The ion heating from viscous damping of the flow associated with tearing modes requires either an excessively high value of the viscosity, or flows confined to layers that are considerably narrower than those observed in experiment.⁶ Furthermore, this mechanism does not predict a cessation of heating when the reversal layer is not present in the plasma, contrary to observations. Stochastic heating was found useful to explain ion heating in Encore.⁵ However, an estimate of stochastic heating in MST, shows that it is too small. The estimate follows Refs. 7 and 11, yielding $\kappa dT_{\parallel}/dt = (m/2)(e/m)^2 \Phi_{\parallel}(0) \sim 10^5$ eV/s, where $\Phi_{\parallel}(0)$ is a square of a time average of the electric field component along the mean magnetic field. This yields a rate that is too small by more than an order of magnitude. Note that most of the ion heating mechanisms mentioned in the previous paragraph generally affect T_{\parallel} differently from T_{\perp} . Evidence shows that while ion heating is isotropic in MST,¹² it is not so in EXTRAP-T2,⁴ where it was found that $T_{\parallel} > T_{\perp}$. Thus, more than one mechanism might be active in RFP plasmas.

In this paper we extend a mechanism suggested earlier by Mattor *et al.*⁸ They showed that global tearing modes driving a cascade to high frequency produce a non Spitzer energy deposition. This work posits an energy budget in which the input power partly sustains the equilibrium (m

$=0, n=0$) and heats the electrons (by finite resistivity), with the remaining energy driving the $m=1$ tearing modes. The tearing modes drive a turbulent energy cascade to higher k , where it is absorbed by the working gas ions and electrons through ion cyclotron damping and electron Landau damping. The viscosity does not play an important role in this mechanism, and it does not rely on collisional equipartition. The cascade has long been regarded as a feature of the RFP fluctuation spectrum. The spectrum shows monotonic decay extending to very high frequencies ($f \sim 1$ MHz). This mechanism is capable, in principle, of producing $T_i > T_e$, however, the amount of heating is sensitive to the spectrum energy at the bulk-ion cyclotron resonance. In MST, the spectrum decay leaves too little energy at the cyclotron resonance to explain observations.

Recent observations in MST suggest that it is worth re-examining this mechanism to include cyclotron resonance heating of impurity ions. It has been discovered that high Z impurities are heated more strongly than bulk ions, implying $T_\alpha > T_i > T_e$. Moreover, a closer look at the measurements in MST (Ref. 1) and ZT-40M (Ref. 3) suggests that heating rates satisfy a similar inequality,

$$\frac{\Delta T_\alpha}{\Delta t} > \frac{\Delta T_i}{\Delta t} > \frac{\Delta T_e}{\Delta t}. \quad (1)$$

The cyclotron resonance occurs at lower frequencies for high Z impurities than it does for hydrogen. In a decaying spectrum this yields higher fluctuation energy at the resonance and stronger ion heating. Consequently it is possible for observed impurity ion heating rates to match theory even if direct cyclotron heating of the bulk ions is too weak. It must then be shown that heating of bulk ions by collisional transfer from the heavier impurity ions fits the observational data.

The observation that impurity ions are more strongly heated than bulk ions suggests there may be a stronger link than previously thought between ion heating in laboratory plasmas and the solar corona. In the solar corona, ions receive more energy than electrons,^{13,14} and radiate or lose energy to the transition region below. The precise physical processes are a subject of current research. Data from the Solar and Heliospheric Observatory (SOHO) show that the temperature of the minority ions exceeds the proton temperature.^{13,14} The temperature perpendicular to the magnetic field also exceeds the parallel temperature. The temperature anisotropy is suggestive of cyclotron damping, although the fluctuation frequencies are lower than the cyclotron resonance frequency. Cyclotron resonance heating rates for impurity ions have nonetheless been calculated for the solar corona and provide a useful guide for our considerations.

Here we apply this type of analysis to the RFP, assuming that cascade energy is ion-cyclotron damped to heat the impurities. We use the energy budget of Mattor *et al.* to calibrate the total fluctuation energy in the RFP.⁸ A power-law spectrum is assumed, with an index consistent with experiment. A turbulent cascade, which transfers energy to higher wave numbers, is continuously sustained by the large-scale drive of global tearing instability. By extending the analysis

of Mattor to impurity resonances we retain the major idealization of that work. Mattor represented the magnetic fluctuations of the RFP as unbounded Alfvén waves propagating along the mean field, with intensities that decrease with wavenumber according to the observed spectrum. This enabled the use of heating rates calculated in the literature from the simple Alfvénic dispersion relation, $\omega = k_{\parallel} V_A$, as the real part of a consistent limiting root of the plasma dielectric.^{9,15–20} Numerical solution shows that these analytic expressions are reasonable for small k_{\parallel} . However, because the damping is largest for largest k_{\parallel} , we will rely on numerical solutions.

The true experimental situation is sufficiently complicated that we know of no set of consistent approximations that reduces an exact theory to the Alfvén wave idealization of Mattor *et al.* On the other hand, a number of congruences between experiment and this idealization suggest that it is a reasonable heuristic starting point for estimating heating rates. The experimental fluctuations are neither unbounded waves propagating along the mean field, nor the waves of an unbounded turbulent Alfvén-wave cascade (which propagate perpendicular to the mean field). Instead they are nonlinear bound eigenstates of an inhomogeneous plasma, excited by spectral energy transfer. These fluctuations propagate in toroidal and poloidal directions with a phase velocity that appears to asymptote to the Alfvén speed for large wavenumber. This is consistent with MHD fluctuations away from resistive layers. The spectrum is asymmetric in wavenumber space, showing energy depletion in a range that satisfies impurity cyclotron resonances with a parallel propagating Alfvén wave, $\omega = k_{\parallel} V_A = \Omega_\alpha$.²² This is consistent with Mattor's Alfvén wave idealization. On the other hand, the spectrum has $k_{\perp} > k_{\parallel}$, while the limit of the plasma dielectric that gives $\omega = k_{\parallel} V_A$ requires $k_{\perp} < k_{\parallel}$. Finite k_{\perp} introduces coupling to other branches of the plasma dispersion relation. At present nothing is known experimentally about whether such branches are excited in the cascade. Hence we calculate heating rates from the plasma dielectric, taking $k_{\perp}/k_{\parallel} < 1$ as the limit that yields $\omega = k_{\parallel} V_A$ for the wave dispersion. A theory that is more realistic will not only have $k_{\perp}/k_{\parallel} > 1$, but must properly treat the fluctuations as nonlinearly excited, finite width, $\Delta' < 0$, diamagnetic tearing modes subject to the kinetic dissipation of cyclotron resonance. This daunting set of requirements is beyond our present scope, and is deferred to future work.

The observed rise of impurity and bulk ion temperatures resulting in $T_\alpha > T_i > T_e$ immediately after a sawtooth crash leads us to investigate the idea that this inequality may result from collisional energy transfer between anomalously heated impurities and the bulk species, along with direct cyclotron heating of bulk ions. To test this idea we incorporate impurity and bulk cyclotron heating rates into a 0D transport model that includes collisional transfer between species and anomalous energy losses due to turbulence. The calculated equilibration rates are sufficiently rapid (on the order of a millisecond) that collisional transfer between impurity and bulk ions plays a role in observed temperature evolution after a sawtooth crash. The transport model also allows us to consider the effect of collisional equilibration of anisotropic ion

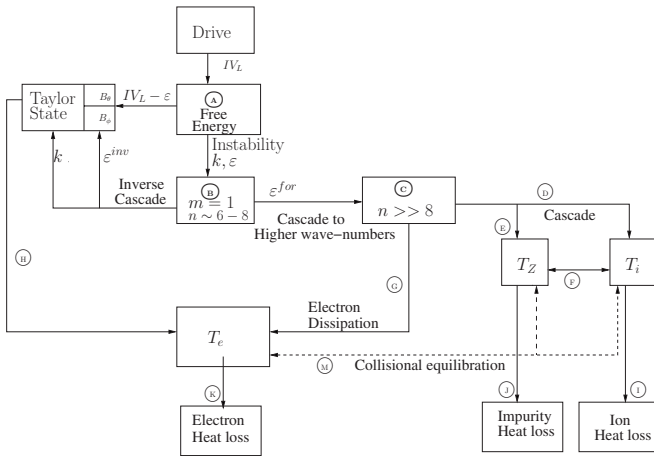


FIG. 1. The energy budget. The energy primarily enters the system as an inductive drive. Available free energy destabilizes the $m=1$ modes, whereupon, a part of the energy cascades to the higher n modes, from where it is picked up by impurities and bulk ions by ion-cyclotron resonance. Here, k is the helicity.

temperatures resulting from the perpendicular nature of cyclotron heating. In these analyses we consider a variety of ion impurity species known to be present in MST discharges. The principal result of this paper is that cyclotron heating of impurities and bulk ions, along with collisional equilibration, yields heating rates that are sufficient to account for the observed rise in impurity and bulk temperatures. Lower density plasmas are found to be hotter and more thermally anisotropic.

This paper is organized as follows. In Secs. II A and II B, we present the energy budget and relevant parameter values for MST, which we take as our typical plasma. In Sec. III we describe three calculations required as inputs to the transport model. Ion heating is estimated by cyclotron damping of Alfvén waves in a cold, isotropic plasma, and is described in Sec. III A. We briefly discuss electron heating in Sec. III B. Conversion of wave energy to thermal energy is described in Sec. III C. Simple collisional transfer processes are examined in Sec. IV. Ion heating and collisional transfer are incorporated into a 0D transport model in Sec. V. This model is used to study temperature evolution under various time-dependent, experimental heating scenarios, such as a sawtooth crash. Conclusions are presented in Sec. VI.

II. ENERGY BUDGET FOR REVERSED FIELD PINCHES

A. Energy budget

In Fig. 1, we illustrate a flowchart of the energy budget for RFP discharges. As with the original formulation,⁸ our adaptation consists of various stages, each with its own sources and sinks. In Fig. 1 each stage has been marked with a circled letter (A, B, C, etc.). Important physical phenomena involved in the energy budget are labeled inside rectangles. The energy and helicity flow are illustrated by the direction of arrows.

Energy is introduced by the inductive drive, appearing as poloidal field energy. This inductive drive sustains the Taylor state and is the source of free energy for unstable tearing

modes (stage A in Fig. 1). The unstable tearing modes have $m=1$, where m is the poloidal wavenumber. After injection into $m=1$ modes, energy participates in a dual cascade process. A part of the energy is carried to the lower wave numbers with the inverse helicity cascade. The rest is carried to the higher wavenumbers as a direct cascade. This branching takes place at B, in Fig. 1. The branching ratio is $\epsilon^{\text{for}}/\epsilon^{\text{inv}}$, where ϵ^{for} is the fraction of energy carried to small scale and ϵ^{inv} is the fraction carried to large scale with helicity. The branching ratio can be easily estimated using arguments in Ref. 8. These arguments consider the helicity required to sustain the equilibrium and calculate the energy ϵ^{inv} carried with that helicity. The remaining cascade energy is ϵ^{for} . This allows the branching ratio to be formulated in terms of the anomalous loop voltage V_L^{anom} , the Spitzer loop voltage V_L^{sp} , and the Taylor state magnetic field configuration. From Eqs. (12) and (17) of Ref. 8, we have

$$\frac{\epsilon^{\text{for}}}{\epsilon^{\text{inv}}} = \frac{V_L^{\text{anom}}}{V_L^{\text{sp}}} \left[\frac{\mu a (J_0^2 + J_1^2) - J_0 J_1}{\mu a (J_0^2 + J_1^2) - 2J_0 J_1} \right], \quad (2)$$

where $J_0 = J_0(\mu a)$ and $J_1 = J_1(\mu a)$ are Bessel functions, a is the minor radius, $\mu = 2.4/a_{\text{rev}}$, and a_{rev} is the reversal radius. From experiments, we know that $V_L^{\text{anom}}/V_L^{\text{sp}} \sim 4-10$ and $\Theta = \mu a/2 \geq 1$. These input values to Eq. (2) lead to the conclusion that for typical parameters (i.e., $V_L^{\text{anom}}/V_L^{\text{sp}} \sim 5$), $\epsilon^{\text{for}}/\epsilon^{\text{inv}} \sim 0.85$. Therefore, more than half of all input energy is available for the forward cascade.

Stage C represents the forward cascade of energy to modes with successively higher values of n , but primarily with $m=1$. This happens through three-wave interactions with the $m=0$ mode. From stage C, there are branches associated with different energy paths into charged particle species through wave-particle resonance processes that remove energy from the cascade. In a homogeneous plasma the cascade would be thought of as an Alfvénic cascade resulting from nonlinear interactions between Alfvén wave packets propagating oppositely along the field of large-scale fluctuations. Because the process is nonlinear, energy is transferred from the large scales ($m=1, n=6-8$) to smaller scales ($m=1, n \geq 8$). As explained earlier, we assume that waves with $n \geq 8$ are Alfvén waves. Our prescription of calculating heating from parallel propagating Alfvén waves results in the same resonant frequency as the waves of a perpendicular cascade if the critical balance hypothesis is satisfied.²³ However, the representation of bound eigenstates by propagating waves is an idealization, and will be replaced with a more realistic treatment in future work. The experimental fluctuation spectrum falls off with wavenumber and has been characterized with a power law $\tilde{B}^2 \propto k^{-\delta}$, where δ is a real number, typically greater than 1. This implies that the modes with higher n values will have lower energy. In this work, we take $\delta=5/3$ for concreteness. The qualitative features of the wavenumber spectrum can be obtained from Fig. 14 of Ref. 1

The high n modes excited in the cascade ultimately exchange energy with particles. This kinetic energy is in turn thermalized by collisions. The stage labeled D marks the energy given to electrons via electron Landau damping

(ELD). The remaining energy is channeled to ions and impurities via ion cyclotron resonance damping (ICR). The ion cyclotron heating occurs in (D) and (E) in Fig. 1. Electron-ion, electron-impurity, ion-impurity collision mechanisms have been included into the energy budget for the sake of completeness. These mechanisms have been labeled as (F) and (M). At (F) we represent the effects of impurity-ion collisions. We assume that impurities, once heated, transfer their energy to the bulk plasma by this method.

The stage (H) represents the resistive electron heating discussed earlier. This is just the Ohmic heating of electrons associated with the equilibrium currents. As shown later, the equilibration of electron temperature is mostly affected by Ohmic heating (H) and transport losses (K). Energy transfer to electrons from electron Landau damping is negligible. The energy transferred to particles can be lost from the plasma through transport, either collisional or anomalous. These losses appear at points (I), (J), and (K) as ion, impurity, and electron heat losses, respectively.

An example of energy distribution within the budget can be gleaned from a sawtooth crash. During a crash in MST, the changes in magnetic energy are much more dramatic than the changes in thermal energy. Within a time of about 100 μ s, the change in magnetic energy is usually 10–15 kJ, while the corresponding gain in thermal energy is only 2–5 kJ. In the same amount of time, the temperature however doubles. Referring to the energy budget, the remaining magnetic energy goes into heating the particles, restoring the Taylor state, and confinement losses. The fluctuations close to the cyclotron frequency will be spontaneously damped to heat the particles, with a rate proportional to the square of the fluctuation level.

B. Experimental parameters

To characterize the plasmas for which we calculate heating rates, we briefly overview parameter values for MST plasmas in which ion heating has been studied. These plasmas have a density of 10^{13} cm $^{-3}$, a magnetic field with a toroidal component on axis of 0.25 T, and equal ion and electron temperatures of 200 eV. These values apply to the period between sawtooth crashes. We do not consider discharges designed to optimize performance, which significantly raise the temperature, density, and plasma beta value. For the parameters quoted above the cyclotron frequency for the majority deuterium species is 1.2×10^7 s $^{-1}$, the Larmor radius is 0.8 cm, and the plasma beta is slightly above 1%. Impurity concentrations are important in the calculation of heating and equilibration rates. Impurity concentrations are not precisely known in MST. The prevalent impurities are carbon (from the wall cover elements) and oxygen (from water contamination). Spectroscopic measurements of Bremsstrahlung radiation allow a direct estimate of Z_{eff} , from which impurity concentrations can be found using the definition $Z_{\text{eff}} = (\sum_{\alpha} n_{\alpha} Z_{\alpha}^2) / (\sum_{\alpha} n_{\alpha} Z_{\alpha})$. The Z_{eff} estimates are in the range 3–4, from which a single impurity of fully stripped carbon would have a concentration between 7% and 10%. For O $^{+5}$ the cyclotron frequency is 0.57 times the cyclotron frequency of deuterium, the working gas ion. The Larmor

radius is 0.31 times the Larmor radius of deuterium. For the MST spectrum, the wavenumber range of significant power, including the cyclotron resonant range, has $k_{\perp} \rho_{\alpha} \leq 0.2$. Impurity collision times are discussed in Sec. IV.

Since the plasma beta is low ($\sim 1\%$), typical Alfvénic phase velocities exceed thermal velocities [$|\omega/k_{\parallel}| \sim V_A = \sqrt{(2/\beta)} V_{\parallel\alpha} \gg V_{\parallel\alpha}$, where ω/k_{\parallel} is the typical phase velocity, and V_A is the Alfvén speed and $V_{\parallel\alpha}$ is the ion thermal speed]. This means the response of the particles is slow compared to typical perturbation time scales, i.e., the plasma wave dielectric may be evaluated in the cold limit. Furthermore, $V_A/c \sim 4 \times 10^{-3}$, where c is the speed of light. Thus in the simplest approximation, we assume $c \gg \omega/k_{\parallel} \gg V_{\parallel\alpha}$. In calculating heating rates collisions may be neglected because $\Omega_{ci} \tau_{ii} \sim 6 \times 10^3$, where Ω_{ci} is the bulk (deuterium) ion cyclotron frequency. This allows us to use a collisionless dielectric tensor.

III. HEATING AND COLLISIONAL TRANSFER IN THE ENERGY BUDGET

A. Alfvén wave damping in an isotropic plasma

Expressions comparable to the following appear in a variety of references.^{18,27,28} Those that are necessary for evaluating the RFP ion-heating physics as stipulated in the energy budget are collected here, and written in a consistent notation. The expressions are based on a straightforward evaluation of the cold plasma dielectric for $k_{\perp}^2 \rho^2 < 1$ and $k_{\perp} < k_{\parallel}$.

The dielectric tensor for an anisotropic, bi-Maxwellian particle distribution in a plasma with several species indexed by α is given by²⁷

$$K_{ij}(\omega, k) = \delta_{ij} + \sum_{\alpha} \frac{\omega_{p\alpha}^2}{\omega^2} \left\{ A_{\alpha} a_{ij} + \frac{\omega^2}{k_{\parallel}^2 V_{\parallel\alpha}^2} b_i b_j + \sum_{s=-\infty}^{s=\infty} z_s^{\alpha} Z(z_s^{\alpha}) \left[A_{\alpha} + \frac{\omega - k_{\parallel} U_{\alpha}}{\omega - s \Omega_{\alpha} - k_{\parallel} U_{\alpha}} \right] \times N_{ij}^{\alpha}(\omega, k, s) \right\}, \quad (3)$$

where $A_{\alpha} = (T_{\parallel\alpha}/T_{\perp\alpha}) - 1$ and $z_s^{\alpha} = (\omega - s \Omega_{\alpha} - k_{\parallel} U_{\alpha}) / (\sqrt{2} k_{\parallel} V_{\parallel\alpha})$, s is an integer that can be either positive or negative, $\omega_{p\alpha}$ is the plasma frequency, Ω_{α} is the cyclotron frequency, and U_{α} is the relative drift velocity along the magnetic field. Hereafter U_{α} will be taken as zero. We have assumed that the plasma has a temperature $T_{\parallel\alpha}$ along the mean magnetic field, which lies in the z -direction. In case the plasma is thermally isotropic, $A_{\alpha} = T_{\parallel\alpha}/T_{\perp\alpha} - 1 = 0$. The wavevector \mathbf{k} is taken to lie in the x - z plane. Hence, $\hat{\mathbf{b}} = (0, 0, 1)$ and $\mathbf{k} = [\sin(\theta), 0, \cos(\theta)]$. The matrix elements of N_{ij} and a_{ij} appearing in Eq. (3) have been defined in Ref. 27. We have used, $N_{11} = e^{-\lambda} \alpha s^2 / \lambda_{\alpha} I_s$ and $a_{11} = 1$. Here, $I_s(\lambda)$ is a modified Bessel function of argument $\lambda = k_{\perp}^2 \rho^2$ and ρ is the ion gyroradius. The function $Z(z)$ is the plasma dispersion function $Z(z) = (1/\sqrt{\pi}) \int_{-\infty}^{\infty} dt \exp(-t^2)/(t-z)$.

Following Refs. 29 and 27, Eq. (3) simplifies the dispersion relation for Alfvén waves to $n_A^2 = K_{11}/\cos^2(\theta)$, where $n_A = ck/\omega$ is the refractive index of Alfvén waves. This can be expressed as (writing $k = k_{\parallel}$)

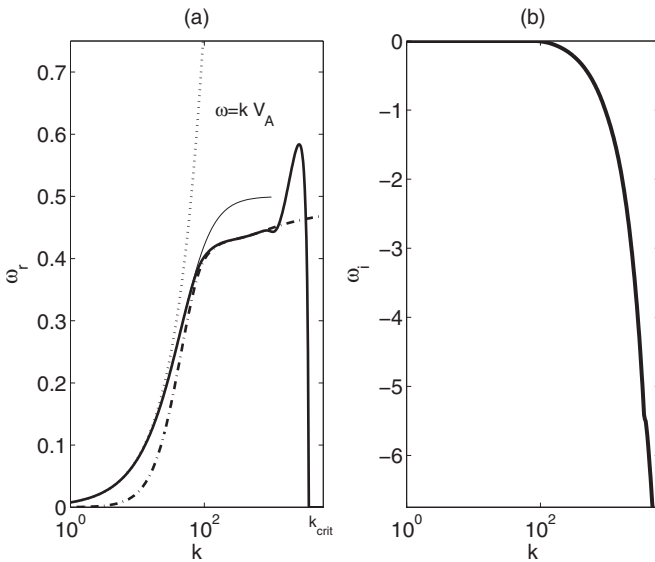


FIG. 2. (a) Normalized real frequency (ω_r/Ω_H) as a function of normalized wavenumber $k = ck/\Omega_H$, obtained from Eq. (4) with $s = \{-1, 0, 1\}$ (solid line); Eq. (4) with $s = 1$ (dash-dotted line); Eq. (10) (thin solid); Eq. (12) with $\lambda = 0$ (dotted line). (b) Normalized damping rate of the wave. Waves with phase velocity $V_{ph} \sim c$ have been ignored.

$$X^3 = \sum_{\alpha} Y \omega_{pH\alpha} P_{\alpha} \sum_{s=-\infty}^{\infty} Z(z_{\alpha}) N_{11}(\alpha, s), \quad (4)$$

where $X = ck/\Omega_H$, $Y = \omega/\Omega_H$, $z_{\alpha} = P_{\alpha}(Y - s\eta_{\alpha})/X$, where $\eta_{\alpha} = Z_{\alpha}/M_{\alpha}$, $P_{\alpha} = c/\sqrt{2}V_{||\alpha}$, $\omega_{pH\alpha} = \omega_{p\alpha}^2/\Omega_H^2$.

Note that Eq. (4) is a nonlinear equation in Y [because of the dispersion function $Z(z_{\alpha})$], therefore, it must be solved numerically for each X . Complete solution of Eq. (4) is obtained using the Muller method²¹ with an initial guess for Y . The complex valued dispersion function in Eq. (4) has been evaluated using the algorithm of Ref. 32. The numerical solution is plotted in Fig. 2 for two different truncations of the summation over s , shown as the heavy solid line and the broken line with dots and dashes. The other two lines are common analytic approximations that will be discussed below. If a single value $s = 1$ is retained in the summation, the solution for the real part of the frequency ω_r asymptotes to $\Omega_{\alpha} = \eta_{\alpha}\Omega_H$ (dot-dashed line). The character of the solution changes significantly if additional values for s are retained in the sum. The heavy solid line shows the result for $s = \{-1, 0, 1\}$. Adding further values of s does not lead to significant changes in the solution. The growth rate is not sensitive to the truncation of the sum over s , and is essentially the same for $s = 1$, $s = \{-1, 0, 1\}$, or less restrictive summations.

The difference in solutions for $s = 1$ versus $s = \{-1, 0, 1\}$ can be understood by examining the large- k asymptotic limit of Eq. (4). In this limit the purely real left-hand side diverges and can only be balanced by the right-hand side if it too becomes real. For $s = 1$ this requirement can be expressed as

$$\arg Y + \arg Z \left[\frac{P_{\alpha}(Y - \eta_{\alpha})}{X} \right] = 0, \quad (5)$$

where $\arg f$ denotes the phase of the complex number f . One solution of Eq. (5) is $\arg Y = -\pi/2$, $\arg Z = \pi/2$, which re-

quires $\omega_r/\gamma \rightarrow 0$ and $Y - \eta_{\alpha} \propto \omega_r + i\gamma - \Omega_{\alpha} \rightarrow i\gamma$, or $\omega_r = \Omega_{\alpha}$. Because ω_r is finite in this solution, $\omega_r/\gamma \rightarrow 0$ implies that $\gamma \rightarrow \infty$, i.e., this solution obtains in the asymptotic limit $k \rightarrow \infty$. This is precisely the behavior of the numerical solution for $s = 1$ (dot-dashed line) of Fig. 2. The complexity of the Z function makes it unlikely that there are other solutions.

For $s = \{-1, 0, 1\}$,

$$X^3 = \sum_{\alpha} Y \omega_{pH\alpha} P_{\alpha} \left\{ Z \left[\frac{P_{\alpha}(Y - \eta_{\alpha})}{X} \right] + Z \left[\frac{P_{\alpha}(Y + \eta_{\alpha})}{X} \right] \right\} = 0. \quad (6)$$

This equation has a solution with $\omega_r = 0$, which can be seen by substituting $\omega_r = 0$ into Eq. (6). For $\omega_r = 0$,

$$\begin{aligned} & Z[P_{\alpha}(Y - \eta_{\alpha})/X] + Z[P_{\alpha}(Y + \eta_{\alpha})/X] \\ &= Z(z_{\alpha}|_{\omega_r=0}) + Z(-z_{\alpha}|_{\omega_r=0})^* \\ &= 2i \operatorname{Im} Z(z_{\alpha}|_{\omega_r=0}), \end{aligned} \quad (7)$$

where the Z function parity property $Z(-a^*) = -[Z(a)]^*$ has been used. With this simplification, Eq. (6) becomes an expression that is solved to obtain the value of γ ,

$$X^3 = -2 \gamma \omega_{pH\alpha} P_{\alpha} \operatorname{Im} Z(z_{\alpha}|_{\omega_r=0}) N_{||}. \quad (8)$$

The condition $\omega_r = 0$ is a critical part of the solution because it guarantees that the right-hand side of Eq. (8) is real. It must also be positive, and that requires $\operatorname{Im} Z(z_{\alpha}|_{\omega_r=0}) > 0$, or roughly, $-\gamma > \Omega_{\alpha}$. Note that this root allows a range of γ values provided $\omega_r = 0$. The value of γ is determined by Eq. (8), which requires that $\gamma \operatorname{Im} Z \rightarrow \infty$ as $X^3 \rightarrow \infty$. This is the behavior evident in the heavy solid line of Fig. 2. Note that this solution is nonresonant once ω_r approaches 0. The notion of propagating Alfvén waves is incompatible with $\omega_r = 0$; hence, we will cut off the sum over k at the value where $\omega_r = 0$. It is clear from this analysis that the solution with the truncation to $s = 1$ does not have $\omega_r = 0$ because it does not include the conjugate pairing of Z functions. Obviously, less restrictive truncations with $s = \{-m, -m+1, \dots, -1, 0, 1, \dots, m-1, m\}$ retain the conjugate pairings and therefore retain the solution with $\omega_r = 0$. While the solution with $s = 1$ happens to fit common analytic approximations, its asymptote of $\omega_r \rightarrow \Omega_{\alpha}$ is an artifact of dropping the crucial conjugate pairing with $s = -1$.

We now compare the solutions with common analytic approximations. An approximation that is appropriate for the cold plasma limit (which is well satisfied by the numerical solution) and small damping rates ($\gamma \ll \omega_r$) can be easily derived from Eq. (4).

For this limit, we use the asymptotic expansion for $z > 1$: $Z(z) \approx -z^{-1}(1 + 1/2z^2) + i\sigma\sqrt{\pi}\exp(-z^2)$, where $\sigma = 2$. We include only the effects of the fundamental harmonic frequencies (i.e., $s = -1, 0, 1$). The real terms reduce to the cold plasma dielectric tensor, which is written as

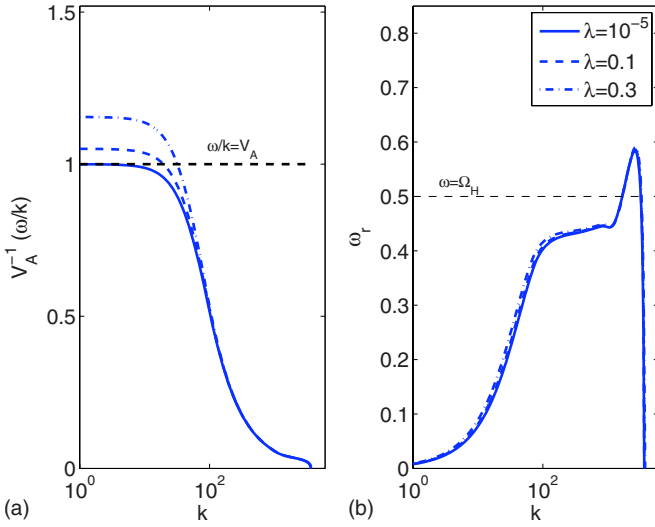


FIG. 3. (Color online) (a) Normalized phase velocity and (b) real frequency as a function of the parallel normalized wave-number k for different $\lambda = k_{\perp}^2 \rho_i^2$.

$$K_{11}^{\text{cold}} = \frac{c^2 k^2}{\omega_r^2} = 1 + \sum_{\alpha} \frac{\omega_{p\alpha}^2}{\Omega_{\alpha}^2 - \omega_r^2} \frac{2e^{-\lambda} I_1}{\lambda_{\alpha}}. \quad (9)$$

Ignoring the coupling to the electromagnetic wave ($\omega_r = ck$) and assuming $k_{\perp}^2 \rho^2 = \lambda \rightarrow 0$,

$$K_{11}^{\text{cold}} = \frac{c^2 k^2}{\omega_r^2} = \sum_{\alpha} \frac{\omega_{p\alpha}^2}{\Omega_{\alpha}^2 - \omega_r^2}. \quad (10)$$

The above cited real part of the dispersion relation is illustrated in Fig. 2 as the thin solid line. The imaginary part (the total damping rate γ_{ion} , summed over all species) is given by²⁷

$$\gamma_{\text{ion}} = \sum_{\alpha} \sqrt{\frac{\pi}{8}} \frac{\omega_{p\alpha}^2}{k_{\parallel} V_{\parallel\alpha}} \exp\left[-\left(\frac{\omega_r - \Omega_{\alpha}}{\sqrt{2} k_{\parallel} V_{\parallel\alpha}}\right)^2\right]. \quad (11)$$

The above expressions are strictly valid only for low damping rates ($|\omega_r| < |\Omega_i|$ and $\gamma_{\text{ion}} \ll \omega_r$). Since γ_{ion} is proportional to $\exp[-(\omega_r - \Omega_{\alpha})^2 / (\sqrt{2} k_{\parallel} V_{\parallel\alpha})^2]$, the term $R_{\alpha} = |(\omega - \Omega_{\alpha}) / (k_{\parallel} V_{\parallel\alpha})|$ must be small to avoid exponentially small cyclotron damping. The condition $R_{\alpha}^2 / 2 \leq 1$, implies the resonance condition $\omega - \Omega_{\alpha} \leq \sqrt{2} k_{\parallel} V_{\parallel\alpha}$. Equation (10) can be further simplified in the special case of low frequency ($\omega \ll \Omega_{\alpha} \ll \omega_{p\alpha}$), wherein we recover the shear Alfvén wave with the usual dispersion relation $\omega^2 = k_{\parallel}^2 V_A^2$. In Fig. 2, this is indicated as a dotted line.

The parametric variation of the solution for various $k_{\perp}^2 \rho_i^2$ and density n is illustrated in Fig. 3. Changing either of these parameters does not effect the dispersion or damping at high k . The critical wavenumber k_{crit} (k at $\omega_r \sim 0$) also remains unchanged. The only observable changes happen at the low k and low frequency limit. As illustrated in Fig. 3, the phase velocity increases with $\lambda_{\alpha} = \lambda$. A simple explanation of this can be obtained from Eq. (9). For $\omega_r \ll \Omega_{\alpha}$, we have

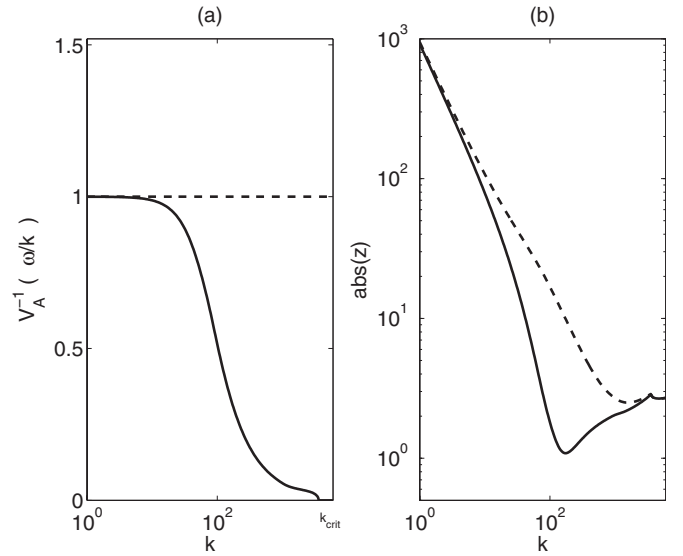


FIG. 4. (a) Normalized phase velocity $V_A^{-1} \omega_r / k$. We have only considered the wavenumber sub-range with $\omega_r \neq 0$. (b) Resonance terms $z_{\pm} = (\omega \mp \Omega_{\alpha}) / (k V_r)$ vs normalized frequency.

$$\frac{c^2 k^2}{\omega_r^2} = \sum_{\alpha} \frac{\omega_{p\alpha}^2}{\Omega_{\alpha}^2} \left[\frac{2e^{-\lambda} I_1}{\lambda} \right], \quad (12)$$

which further reduces to $\omega = k_z V_A / \sqrt{2e^{-\lambda} I_1(\lambda) / \lambda}$, since $\sum_{\alpha} \omega_{p\alpha}^2 / \Omega_{\alpha}^2 = c^2 / V_A^2$. Thus in a low frequency regime, the Alfvén wave dispersion is modified. Now $\sqrt{2e^{-\lambda} I_1(\lambda) / \lambda}$ is a monotonically decreasing function of λ , therefore, the normalized phase velocity $V_A^{-1} \omega_r / k$ increases on increasing λ .

In Fig. 2 we also plot the real frequency, solved as the root of Eq. (10), for a pure plasma (thin solid line). The dotted line corresponds to $\omega = k_{\parallel} V_A$. We have assumed a pure helium plasma with $B_o = 0.4$ T and $n_i = 3.46 \times 10^{18} \text{ m}^{-3}$. The initial temperature for each species is assumed to be about 540 eV. Note that in this figure the scale of the x -axis is logarithmic so the Alfvén wave dispersion relation does not appear as a straight line. In the range $ck_{\parallel} / \Omega_H \ll 1$, where ω / Ω_H is also small, the complete dispersion relation is close to that of the Alfvén wave.

Using the parameters of Fig. 2(a), the variation of z_{\pm} is illustrated in Fig. 4(b). In this figure, the condition ($z_{\pm} \geq 1$) is satisfied implying the plasma is cold.

B. Electron Landau damping

Apart from heating the ions via ion cyclotron damping, the energy cascade can also lead to electron heating via ELD as described in the energy budget. An estimate of this is important because it may help explain why ions tend to be so hot in RFP plasmas. To argue our point we assume the same conditions on wave properties used previously to estimate the electron dissipation and thus the branching ratio at point C. These correspond to $\gamma < \omega_r$ and $\omega_r < \omega_{\alpha}$, where simple analytic formulas and the numerical solution are in reasonable agreement. For ELD under the wave conditions assumed throughout, the dispersion relation can be generalized from Eq. (3) by including the term K_{33} as in Ref. 27,

$$\gamma = -\sqrt{\frac{\pi}{8}} \left(\frac{m_e}{m_i}\right)^{1/2} k_x^2 \frac{k_{\parallel} V_A^2 V_s}{\Omega_i^2} \exp(-(z_o^e)^2), \quad (13)$$

where $V_s = (m_e/m_\alpha)V_e$. The above result is similar to Eq. (2.265) of Ref. 27. The above approximation does not include any cyclotron resonance effects ($\omega < \Omega_i$), contributions from minority species, or finite Larmor radius effects ($k\rho \ll 1$). If effects of a finite λ_{De} are retained, the real frequency is slightly modified as $\omega^2 = k_{\parallel}^2 V_A^2 (1 + k_{\parallel}^2 V_s^2 / \Omega_i^2)$, which is like the usual Alfvén wave in the limit of small k_x .

The above discussion relates to the dynamics at branch point © in Fig. 1. The ion cyclotron part is specific to ④ and ⑤ while the electron Landau damping part is specific to ⑥. The branching ratio at point © can thus be calculated. For this, we simply take the ratios of the two damping rates computed above [Eqs. (11) and (13)], yielding

$$\frac{\text{Energy on ④ and ⑤}}{\text{Energy on ⑥}} = \frac{\varepsilon^{\text{ion}}}{\varepsilon^{\text{electron}}} = \frac{\gamma_{\text{ICR}}}{\gamma_{\text{ELD}}}. \quad (14)$$

The above equation neglects any energy that couples across the narrow ICR resonances. It is possible that this fraction may end up as electron or ion heat and is not accounted for. This equation also assumes that the heating rate is directly proportional to the damping rate of these waves, and that the level of fluctuations is the same at both frequencies. This is justified since we are looking at that fraction of electron Landau damping that is important on Alfvén time scales. The branching ratio is given by

$$\frac{\gamma_{\text{ELD}}}{\gamma_{\text{ICR}}} = \left(\frac{m_e}{m_\alpha}\right)^{1/2} k^2 \lambda_D^2 \sqrt{\frac{T_\alpha}{T_e}} \ll 1. \quad (15)$$

From this ratio we conclude that unless $k^2 \lambda_D^2 \gg 1$, the most important mechanism for heating the electrons is not electron Landau damping.

In a similar fashion, we can also compute the relative branching ratio between paths ④ and ⑤ (heating of bulk ions and a single impurity),

$$\frac{\varepsilon^{\text{ion}\alpha}}{\varepsilon^{\text{ion}\beta}} = \frac{\gamma^{\text{imp}\alpha}}{\gamma^{\text{imp}\beta}} = \left(\frac{Z_\alpha}{Z_\beta}\right)^2 \left(\frac{\mu_\beta}{\mu_\alpha}\right)^{1/2} \left(\frac{n_\alpha}{n_\beta}\right) \left(\frac{T_\beta}{T_\alpha}\right)^{1/2}. \quad (16)$$

Here, μ_α is the ion mass expressed in units of proton mass, Z_α is the charge state, and T_α is the temperature of species α expressed in eV. The above expression neglects the effect of the term $\exp[-(R_\alpha^2 - R_\beta^2)]$, which may play an important role away from resonance, and the resonant wavenumber.

This shows that the heating of a species is proportional to the square of its charge state. It also shows ion heating $\varepsilon^{\text{ion}\alpha}$ is directly proportional to impurity density n_α . In the mobile limiter experiments of HBTX-1B,^{30,31} it was found that when the limiter was inserted into the plasma, the loop voltage increased with the limiter insertion distance, as did the ion temperature. A partial explanation of those experiments can be made on the basis of the energy budget through two effects. First, an increase of loop voltage implies a higher energy source in the turbulent cascade (at branch point ① shown in Fig. 1). This means that more energy can be channeled to ion or electron heat. Furthermore, as the

limiter is inserted, the impurity concentration n_α increases (through sputtering). Thus from Eq. (16), $\varepsilon^{\text{ion}\alpha}$ increases, leading to a higher ion temperature. Note that we have not included the possibility that a species may not be exactly resonant since the damping rate also depends upon the ratio $\exp(-R_\alpha^2)/\exp(-R_\beta^2)$. (If $R_\alpha^2/2 \sim 1$, it implies the resonance condition $\omega - \Omega_\alpha \approx \sqrt{2}k_{\parallel}V_{\parallel\alpha}$ is met.) This ratio changes the number of particles in the tail of the distribution function that can interact with the waves. Note that even if the e/m ratio is the same for two different species, the temperatures will ultimately be different. This is because (i) the damping rate does not simply depend upon the e/m ratio, and (ii) species with the same e/m ratio can still have different values of R_α . Finally, to be able to make the above observations about simple dependencies, we have assumed typical temperature values rather than computing consistently from a transport model.

C. Wave to thermal energy conversion

To model temperature evolution driven by the cyclotron absorption we must estimate the increase in perpendicular thermal energy of each absorbing species through the wave damping rates associated with the plasma dielectric tensor. We focus first on the resonant conversion of wave energy to thermal energy. We assume homogenous turbulence in a torus of major radius R and minor radius a . The boundary conditions are periodic on a scale much larger than the scale of the turbulence. Then we have

$$n \frac{\kappa d\tilde{T}}{dt} = Q_{\perp} = \frac{1}{(\pi a^2)(2\pi R)} \int_0^{k_{\text{crit}}} \omega_i(k/k_0)^{-\delta} \left(\frac{\tilde{B}^2}{2\mu_0}\right) (4\pi k^2) dk, \quad (17)$$

where \tilde{T} is the perpendicular temperature and Q_{\perp} is the ion cyclotron heating rate. The term ω_i is the damping rate of the wave, e is the charge, and $(k/k_0)^{-\delta}$ models the falloff in the magnetic field fluctuation spectrum. We have assumed $\delta = 5/3$. This expression equates the change in thermal energy with the Joule heating ($\hat{J}\hat{E}^*/2$), where \hat{J} is the kinetic charged particle (current) response to the wave electric field as calculated from the dielectric tensor.

As a special case of a one dimensional periodic box with a discrete number of mode k_n , we would have

$$n\kappa \frac{dT}{dt} = \frac{1}{4L} \text{Re} \left(\int_{-L}^L \hat{J} \cdot E^* dx \right) = \frac{1}{4} \sum_{n=-\infty}^{\infty} (\hat{J}_n \cdot E_n^* + \hat{J}_n^* E_n). \quad (18)$$

This expression generalizes the results of Eq. (7.18) of Ref. 33 since it includes a large number of modes. From Maxwell's equations, we have $\hat{J}_n = \varepsilon_0 E_n (k_n c^2 - \omega^2) / i\omega$, where $k_n = n\pi/L$ is the parallel wavenumber k_{\parallel} in the box. Substituting and simplifying,

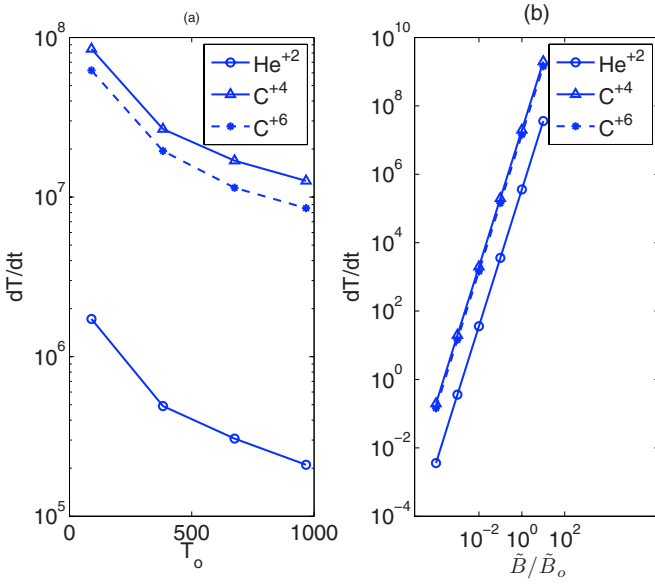


FIG. 5. (Color online) (a) Heating as a function of temperature. Note that the heating mechanism is ineffective at high temperatures. (b) Heating rate as a function of magnetic field fluctuations ($B_0=3\times 10^{-7}$). Note that for small magnetic field fluctuations, the heating is quite low.

$$n\kappa \frac{dT}{dt} = Q_{\perp} = - \sum_{n=-\infty}^{\infty} \left(\frac{\varepsilon_0 E_n E_n^*}{2} \right) \gamma \left(\frac{k_n^2 c^2}{|\omega|^2} + 1 \right). \quad (19)$$

The last bracketed term consists of two parts. The first part $\gamma(\varepsilon_0|E|^2/2)(k_n^2 c^2/|\omega|^2)$ is the change in inductive electric field energy. For simplicity, we refer it as $\gamma(|\tilde{B}_n|^2/2\mu_0)$, where $|\tilde{B}_n|^2$ is the magnetic field fluctuation level. The second part $\gamma(\varepsilon_0|E|^2/2)$ is the contribution from Maxwell's displacement current. For illustration, let us momentarily ignore the first part. The result is similar to Eq. (8) of Ref. 18, provided we assume $R_{\sigma} \ll 1$. The numerical solution of this equation is illustrated in Fig. 3 of Ref. 18. The typical densities used there are $\sim 10^{13} \text{ cm}^{-3}$, close to the parameter regime of MST. In Fig. 3 of Ref. 18, the temperature rises by a factor of 10 in about 100 μs . Of course this illustration ignores the term $k_n^2 c^2/|\omega|^2$, which is orders of magnitude larger for waves whose phase velocity is well below c . (See the x -axis of Fig 2 of Ref. 18, where $kc/\Omega \sim 100\text{--}1000$.) Consequently, the predicted heating increases by a factor of $10^4\text{--}10^5$. These increases are much larger than those of MST because we have ignored for the moment the various loss channels of the energy budget.

In Fig. 5, we illustrate the parametric variation of the heating rate dT_{α}/dt calculated from Eq. (17) as a function of the level of magnetic field fluctuations [Fig. 5(b)] and temperature [Fig. 5(a)]. Note that the heating rate is a very strong function of both these parameters. The x -axis in Fig. 5(b) is a measure of the low frequency fluctuations in the system. For a RFP, this corresponds to the typical fluctuation level for lower frequency tearing modes $\omega < 0.2 \text{ MHz}$ (for example see Fig. 14 of Ref. 1). Note that in this model we have also assumed $(\varepsilon_0|\tilde{E}|^2/2)(k^2 c^2/|\omega|^2) \sim |\tilde{B}|^2/2\mu_0$.

The ion heating mechanism detailed in this paper does not produce appreciable ion heating in tokamaks. The typical

level of fluctuation in tokamaks is usually $\tilde{B}/B_0 \sim 10^{-5}\text{--}10^{-4}$. This gives a heating rate that is too low and easily dominated by confinement losses. In the RFP, magnetic fluctuations are usually larger ($\tilde{B}/B_0 \sim 10^{-3}\text{--}10^{-1}$). In this situation the total heating is approximately $10^6\text{--}10^8 \text{ eV/s}$. This becomes an important contribution even before a crash. While the RFP confinement time is small ($\sim 1 \text{ ms}$) it is not orders of magnitude smaller than the tokamak confinement time. However, magnetic fluctuations are orders of magnitude larger. Thus, as illustrated in Fig. 5(b), anomalous ion heating from magnetic fluctuations appears to be significant only for the RFP. Figure 5(a) indicates that the anomalous ion heating mechanism described herein is a strong function of temperature. At higher temperatures, the heating decreases. Therefore the present mechanism is only significant at low temperatures. This mechanism would not be expected to produce significant ion heating in a reactor plasma.

IV. COLLISIONAL TRANSFER PROCESSES

The primary diagnostic for ion heating in MST is the measurement of ion temperatures. Equation (17) describes temperature evolution driven by ion cyclotron heating, but does not account for the loss channels of the energy budget. In this section we account for collisional transfer between impurities and the bulk ions and examine the rates of transfer for MST parameters.

When the plasma is isotropic and there is no relative drift between the various species the thermal equilibration is described by²⁴

$$\left. \frac{dT_{\alpha}}{dt} \right|_{\text{Collisions}} = \sum_{\beta} \overline{\nu_{\epsilon}^{\alpha\beta}} (T_{\beta} - T_{\alpha}), \quad (20)$$

where $\overline{\nu_{\epsilon}^{\alpha\beta}}$ is given in cgs units by²⁴

$$\overline{\nu_{\epsilon}^{\alpha\beta}} = 1.8 \times 10^{-19} \frac{(m_{\alpha} m_{\beta})^{1/2} Z_{\alpha}^2 Z_{\beta}^2 n_{\beta} \lambda_{\alpha\beta}}{(m_{\alpha} T_{\alpha} + m_{\beta} T_{\beta})^{3/2}} \text{ s}^{-1}. \quad (21)$$

Using the isotropic equations [Eqs. (20)], we test the hypothesis that a small concentration of hot impurities is sufficient to efficiently transfer energy to the bulk plasma. For this purpose we have numerically solved Eq. (20) for a contaminated plasma for the following parameters. The bulk species is H_1^{+1} (with density $n_1 = 1 \times 10^{13} \text{ cm}^{-3}$) and the impurities are C_{12}^{+4} ($n_2 = 0.2 \times 10^{13} \text{ cm}^{-3}$), C_{12}^{+5} ($n_3 = 0.1 \times 10^{13} \text{ cm}^{-3}$), O_{16}^{+5} ($n_4 = 0.02 \times 10^{13} \text{ cm}^{-3}$) and O_{16}^{+6} ($n_5 = 0.03 \times 10^{13} \text{ cm}^{-3}$) so that $n_e = \sum_{\alpha} n_{\alpha} Z_{\alpha} = 2.58 \times 10^{13} \text{ cm}^{-3}$. This means that $n_1/n_e = 0.387$, $n_2/n_e = 0.077$, $n_3/n_e = 0.038$, $n_4/n_e = 0.007$, $n_5/n_e = 0.011$, and $Z_{\text{eff}} = \sum_{\alpha} n_{\alpha} Z_{\alpha}^2/n_e = 3.2$. The assumed initial temperatures ($T_{\alpha}^{\text{initial}}$) in units of eV were $T_1 = 30$, $T_2 = 300$, $T_3 = 260$, $T_4 = 350$, $T_5 = 600$. In this test, we assume that a single minority species [here O^{+6}] has a high temperature at $t=0$. For $\lambda=16$, these parameters imply $\overline{\nu_{\epsilon}^{\alpha\beta}} = 2 \times 10^3 \text{ s}^{-1}$. The dynamical system was allowed to evolve until an equilibrium was reached. The results of this test are illustrated in Fig. 6(a). In the final state, the bulk ion temperature (H^{+1} in this case) increases by a large amount (roughly a factor of 3, i.e., 100 eV in about a hundred microseconds). Furthermore, the hot impurity cools down to the

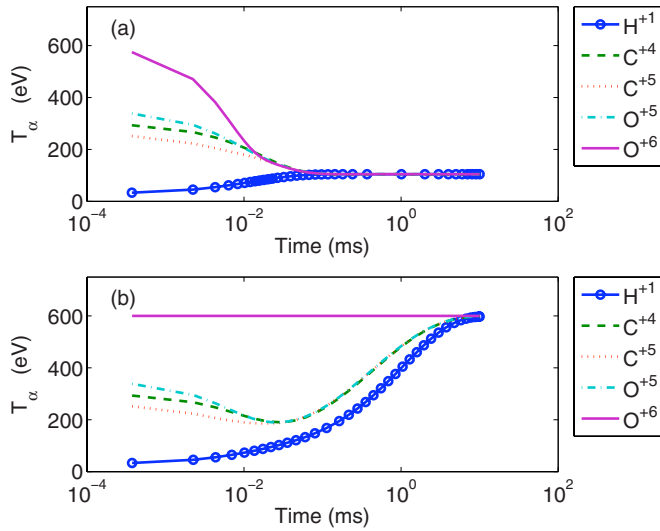


FIG. 6. (Color online) Equilibration of multiple species. (a) Relaxation with a hot impurity (O^{+6}) at $t=0$; (b) Relaxation with one species (O^{+6}) continuously heated. Temperatures were assumed isotropic.

same temperature. Sawtooth crash time scales in MST are on the order of a ms, while the time between crashes is tens of ms. We conclude that collisional equilibration of different species is important in MST, and that impurities are an important heating source for the bulk plasma species.

Between sawtooth crashes the temperatures are essentially stationary. Ion cyclotron heating continues at a lower level because magnetic fluctuations are still present at a lower level. In this situation the steady state is ultimately governed by the irretrievable loss of heat due to transport out of the plasma. If impurity heating exceeds bulk heating, and $T_{c\alpha} > T_i$ transiently (at some arbitrary initial time), the bulk ion species will equilibrate collisionally with the hotter impurity, and both will have elevated temperatures relative to a situation without ion cyclotron heating. Such a scenario is illustrated in Fig. 6(b). We assume a plasma that is a mixture of several species, most of them with low concentrations. The bulk ions are H^{+1} , and are assumed to be the coolest ion species. In this picture, one of the species, (O^{+6}), is presumed to be maintained at a high constant temperature by some unspecified, external mechanism. It can be seen that the other species are heated until equilibrium is reached. The equilibration time is on the order of a ms.

V. THERMAL EVOLUTION

We now assemble the remaining parts of the whole energy budget to create a system of OD equations for temperature evolution. We include transport losses, and assume, as a simplification, that confinement times are constant. Obviously, in non steady state systems, there is variation. For example, during a sawtooth crash, the confinement times evolve through their dependence on the changing magnetic field, safety factor q , temperature, density, and gradients in these quantities. In MST, electron heat confinement deteriorates markedly during a crash, leading to a transient dip in

electron temperature. This fact can also be used to argue that electron-ion collisions are not particularly important for heating ions in these situations.

In constructing the temperature evolution equations we consider first the situation in which perpendicular and parallel temperatures are roughly equal. This is the situation that has generally been reported in MST. However, as cyclotron heating is a perpendicular energy source, we will subsequently examine anisotropic sources and anisotropic temperature evolution.

A. Isotropic temperatures

The temperature evolution equation is given by

$$\frac{d\kappa T_\alpha}{dt} = \sum_\beta \overline{v_e^{\alpha/\beta}} (\kappa T_\beta - \kappa T_\alpha) + \sum_\beta \overline{v_e^{\beta/e}} (\kappa T_e - \kappa T_\beta) + Q_\perp - \frac{\kappa T_\alpha}{\tau_{c\alpha}}. \quad (22)$$

This is a system of several equations where α is an index for each species with temperature T_α . The first term here is the ion-ion equilibration term. Summing over α , this term makes no net contribution to the increase or decrease in the total thermal energy of the particles. The next term is the electron-ion collision term. Like the previous term, it makes no net increase or decrease in the total thermal energy of the particles. The third term is the ion cyclotron damping term. This term is the most important heating term in our model. Finally, the last term describes confinement loss modeled as a linear term with a constant energy confinement time.

If we write an energy evolution equation for the electrons we have

$$\frac{d\kappa T_e}{dt} = \frac{e^2 E^2 \tau_{ei}}{m_e} + \sum_\beta \overline{v_e^{\beta/e}} (\kappa T_\beta - \kappa T_e) + Q_e - \frac{\kappa T_e}{\tau_{ce}}. \quad (23)$$

In this expression the first term refers to direct Ohmic heating, and the second term is the collisional energy exchange between electrons and ions. Note that the sum of this and the corresponding term in the ion equation is zero (i.e., equilibration). The next term represents the heating of electrons by electron Landau damping. The final term is the loss term and leads to saturation. Here, the parameter τ_{ce} models electron confinement during a crash. As mentioned earlier, it has been assumed to be a constant. The coupling between Eq. (22) and Eq. (23) is weak since collisions are too infrequent. In this work, the physics of branch point \textcircled{B} allows us to assume dynamics of the cascade and particle heating is a constant fraction $\varepsilon^{\text{for}}/\varepsilon \sim 0.5$ of the rest of the power balance. We can also compare the above result with previous calculations of the dielectric response of the plasma near the ion cyclotron frequency by Svidzinski.³⁴ These results differ by a constant factor.

B. Anisotropic temperatures

In a strong external magnetic field, ions experiencing cyclotron heating predominantly gain energy in the perpendicular direction. Macroscopically, the energy deposition rate

is much higher in the perpendicular direction. The collision cross sections, which are velocity dependent, can no longer be assumed to be isotropic.

Consider ion velocity distributions that are not isotropic but are bi-Maxwellian characterized by two temperatures T_{\parallel} and T_{\perp} . In the simplest approximation, we can assume a bi-Maxwellian distribution which retains its shape on ion cyclotron heating time scales. On collisional time scales, we assume that T_{\parallel} and T_{\perp} evolve, but still uniquely characterize the distribution function. We have also assumed that $T_{\parallel\alpha}$, $T_{\perp\alpha}$, and n_{α} are all independent of x , y , and z . The general collisional momentum and energy transport terms for interpenetrating bi-Maxwellian distributions were first computed by Barakat and Schunk,²⁵ and later improved and applied to the solar corona models by several authors.²⁶ The model used here is based on Eqs. (1) of Cranmer *et al.*²⁶ To arrive at the equations below, we have assumed that all species (labeled by the index i) drift together with the same velocity (i.e., $u_i = u$), and thus Eq. (1) of Ref. 26 can be transformed to an inertial frame moving with that velocity. We assume the electron temperature remains isotropic because of (i) the high electron collision frequency (e.g., in MST the electron-electron collision frequency satisfies $\tau_{ee} \sim 100\tau_{ii}$, where τ_{ii} is a typical deuterium-deuterium collision time); (ii) high electron cyclotron frequency ($\omega \ll \Omega_{ce}$); and (iii) small Landau damping ($|\omega - k \cdot v| \gg 1$). The equations we have used are

$$\frac{1}{2} n_{\alpha} \kappa \frac{\partial T_{\parallel\alpha}}{\partial t} = \sum_p [C_{\parallel ap} (T_{\parallel p} - T_{\parallel\alpha}) + m_p J_{\parallel ap}], \quad (24)$$

$$n_{\alpha} \kappa \frac{\partial T_{\perp\alpha}}{\partial t} = Q_{\perp\alpha} + \sum_p [C_{\perp ap} (T_{\perp p} - T_{\perp\alpha}) + m_p J_{\perp ap}], \quad (25)$$

where n_{α} is the ion number density, m_p is the mass of species p , and $Q_{\perp\alpha}$ is the ion cyclotron-resonant heating rate. The coefficients $C_{\parallel ap}$ and $C_{\perp ap}$ govern the collisional energy exchange between ions in the absence of flows. These terms only lead to equilibration between several species (i.e., no isotropization). The terms $m_p J_{\parallel ap}$ and $m_p J_{\perp ap}$ describe Joule heating and isotropization from collisions. In the special case of a pure plasma (i.e., just one species in the above equation), the terms $J_{\parallel ap}$ and $J_{\perp ap}$ lead to a collisional equilibration between T_{\parallel} and T_{\perp} . Expressions for m_p , $C_{\parallel ap}$, $C_{\perp ap}$, $J_{\parallel ap}$, and $J_{\perp ap}$ can be found in Ref. 26.

Confinement losses are modeled using approximate confinement times $\tau_{c\parallel\alpha}$ and $\tau_{c\perp\alpha}$ for ions and impurities, and τ_{ce} for electrons,

$$\left. \frac{dT_{\perp\alpha}}{dt} \right|_{\text{losses}} = -\frac{T_{\perp\alpha}}{\tau_{c\perp\alpha}}, \quad \left. \frac{dT_{\parallel\alpha}}{dt} \right|_{\text{losses}} = -\frac{T_{\parallel\alpha}}{\tau_{c\parallel\alpha}}, \quad (26)$$

$$\left. \frac{dT_e}{dt} \right|_{\text{losses}} = -\frac{T_e}{\tau_{ce}}. \quad (27)$$

Consistent with the weak temperature anisotropy of MST we will use a heating rate $Q_{\perp i}$ calculated from ion cyclotron damping in an isotropic plasma, as calculated in Sec. III.

Under the above approximations, we study the evolution of Eqs. (24) and (25) until an equilibrium is reached. The system is initiated with a low initial temperature. These cal-

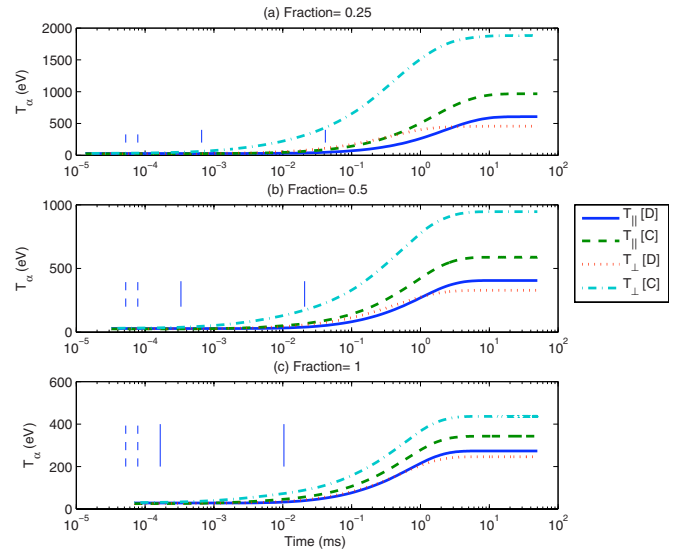


FIG. 7. (Color online) Ion temperature as a function of time for various densities. The densities used in each of the above figures are $n_D = \text{Fraction} \times n_{D0}$ and $n_C = \text{Fraction} \times n_{C0}$, where $n_{D0} = 1 \times 10^{13} \text{ cm}^{-3}$ and $n_{C0} = 0.1 \times 10^{13}$. Note that as density is decreased, the ion temperature increases. The solid vertical line represents typical collisional time scales $1/\nu_i$ and the dashed lines are $\sim 1/\Omega_{ci}$.

culations are summarized in Fig. 7 for different values of the density. The bulk species is D^{+1} and the impurity is C^{+4} . The four initial temperatures are taken in the range 26–28 eV but not exactly the same to ensure finite temperature equilibration terms at $t=0$. Note that as density is decreased, ion temperature increases as observed in experiments. For example, Rostagni recently surveyed some confinement results on RFP machines, particularly the density dependence of ion temperature.³⁵ Observations in Fig. 7 agree qualitatively with Fig. 3 of Ref. 35. Note that a higher density plasma tends to be more isotropic. The anisotropy of temperature T_{\parallel}/T_{\perp} increases as density is decreased. Such a prediction finds favorable evidence from experiment, particularly Ref. 4, in which the density dependence of anisotropy was studied on the EXTRAP-T2 machine.

We analyze the effect of the transient increase of fluctuating magnetic field associated with a sawtooth crash. At the crash, both core and edge modes are excited, and ion heating is strong. The crash has been simulated by using the periodic function $\tilde{B}^2 = A_o \exp[-r \sum_i \sin(tk_i)/k_i]$, where r and A_o are constants. An actual sawtooth oscillation may have different rise and fall times. Nevertheless, several essential features can be illustrated in this way by using a pulse with a rise time of a few hundred microseconds and a peak value of $\tilde{B} \sim 3 \times 10^{-7} \text{ T}$. This approximate value is consistent with experimental spectra in the ion cyclotron frequency range (see Fig. 14 of Ref. 1). Such a form (normalized to 1 for illustration) is indicated in Fig. 8(c) by the thin line. A system of two species has been allowed to relax under the periodic drive and the transients ignored. Figures 8(a)–8(c) are evolutions of parallel and perpendicular temperatures for increasing density. This figure has several notable features: (i) heating increases with decreasing density, (ii) the heating rate of impurities is higher than that of the bulk species, and (iii)

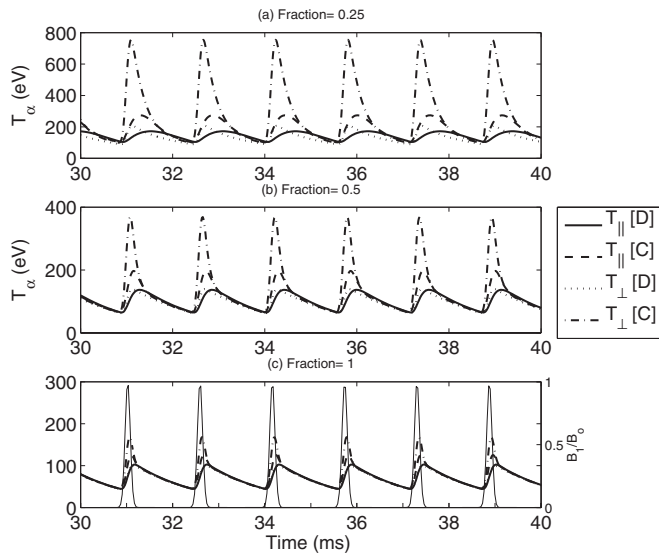


FIG. 8. Ion and impurity heating for three different densities. Note that the heating rate for the impurity is higher than that of the bulk species. The densities used in each of the above figures, $n_D = \text{Fraction} \times n_{D0}$ and $n_C = \text{Fraction} \times n_{C0}$, where $n_{D0} = 1 \times 10^{13} \text{ cm}^{-3}$ and $n_{C0} = 0.1 \times 10^{13}$. The thin solid line is the pulse of the sawtooth crash modeled as $A = A_0 \exp[-r \sum_i \sin(tk_i)/k_i]$.

the magnitude of heating is comparable to experiments. As mentioned in the Introduction, these are the main features of experiments. The impurity temperature rises above the bulk ion temperature, despite the fact that bulk ion growth rates, as seen from Eq. (11), tend to be larger. The growth rates are proportional to density through the $\omega_{p\alpha}^2$ dependence of Eq. (11). As seen from Eq. (22) the time rate of change of temperature is proportional to γ_α/n_α , so the density scaling of $\omega_{p\alpha}^2$ cancels out. The stronger heating of impurities relative to bulk ions comes essentially from the larger wave fluctuation energy at the lower resonant wavenumber.

In the MST, the ion temperature has been reported to be isotropic away from a crash possibly due to thermal equilibration. However in the EXTRAP-T2 plasmas, the parallel temperature is found to dominate the perpendicular temperatures ($T_{\parallel} > T_{\perp}$) for low density plasmas.⁴ This may suggest that some additional parallel heating mechanism is present. However an alternate possibility may be found in Figs. 8. Notice that in this figure, $T_{\perp}(D)$ is lower than $T_{\parallel}(D)$ but $T_{\parallel}(C) < T_{\perp}(C)$. In a complex system like the EXTRAP-T2 where several species are present, it may be possible to have a higher parallel temperature.

VI. SUMMARY AND CONCLUSIONS

Anomalous ion heating in reversed field pinches is not understood despite extensive work on the subject. Recent observations, e.g., $T_\alpha > T_i > T_e$, are difficult to explain using known conventional theories. In this article, impurity ion heating during a sawtooth crash by a cascade of Alfvén waves has been investigated. This mechanism was previously proposed⁸ for anomalous bulk ion heating but met difficulty in explaining bulk ion temperature. In this mechanism, the energy is distributed according to the energy

budget and the branching ratios of Fig. 1. During a sawtooth crash, the energy in the fluctuations increase dramatically. The energy budget dictates that only a part of this energy is available for ion heating (through a cascade of shear Alfvén waves driven at large scale by the unstable global tearing modes). The heavier mass of some species allows them to be gyro-resonant at lower frequencies, where more energy is present in the fluctuations. We have used isotropic and anisotropic heating rates from the plasma dielectric tensor to numerically calculate heating rates. Collisional transfer dynamics are solved using a 0D thermal equilibrium model.

Our simulations reveal several features consistent with experiment. Impurity ions are found to be hotter than the bulk species.¹ The calculated heating rates are sufficient to account for the observed rise in impurity temperatures, provided ions are primarily heated by ion cyclotron resonance. We have computed the various branching ratios that determine relative heating rates of electrons versus the bulk and impurity ions (i.e., electron Landau and ion cyclotron damping). The contribution to total heating from electron Landau damping is small; electrons are heated predominantly by resistive heating. We have shown that if one impurity species is heated to a high temperature, it can collisionally transfer a large portion of its energy to the bulk species, even though the density is low. The energy transfer rate is compatible with rise times of bulk ion temperature in MST after a sawtooth crash. Hot electrons cannot efficiently transfer their energy to the bulk. The above observations can be attributed to the following physical properties: (i) predominantly perpendicular ion cyclotron heating, (ii) density dependence of the Alfvén wave dispersion relation, and (iii) significant amount of fluctuations being present at the impurity cyclotron frequency.

We have also studied the anisotropic relaxation of a contaminated bi-Maxwellian plasma and reproduced several features generally observed in discharges,^{1,4,31,35} particularly those associated with density dependence. We have found that a higher density plasma tends to be more colder and more isotropic. The parallel temperature T_{\parallel} can be significant and comparable to the perpendicular temperature T_{\perp} . This can be attributed to the presence of collisions in the system. The anisotropy of temperature T_{\parallel}/T_{\perp} increases as density is decreased. Furthermore, the model also explains why experiments on HBTX-1B gave a higher temperature³¹ when the limiter was inserted into the plasma.

The model has several limitations based on the assumptions that have been made. Most importantly, it is based on the assumption that parallel propagating Alfvén waves are responsible for the observed ion heating. It assumes $k_{\perp}\rho_i \ll 1$ and $k_{\perp} \ll k_{\parallel}$. It assumes constant confinement time which may not be true in reality. The absolute relative drift between various species is assumed to be negligible. It assumes that parallel heating is negligible. It assumes collisions do not modify the dielectric tensor. The results derived herein will change if k_{\perp} finite is allowed. While testing for such changes will be instructive, it is not clear that they will lead to a more accurate estimate of ion heating in the RFP. This is because refinements to the wave idealization do not address the more

fundamental issue of accurately representing the bound eigenstates of the RFP.

This model also has implications for temperature measurements in experiments. A significant amount of heating implies that the bulk species and impurities are not in equilibrium and therefore spectroscopic measurements of impurity temperature cannot be directly assumed as an estimate for the bulk temperature unless an estimate of bulk heating is made. This observation also implies a limitation of the above model.

ACKNOWLEDGMENTS

This work was supported by the U.S. Department of Energy under Grant. No. DE-FG02–85ER53212.

- ¹E. Scime, M. Cekic, D. J. Den Hartog, S. Hokin, D. J. Holly, and C. Watts, *Phys. Fluids B* **4**, 4062 (1992).
- ²B. Jones and R. Wilson, *Nucl. Fusion Suppl.* **3**, 889 (1962).
- ³R. B. Howell and Y. Nagayama, *Phys. Fluids* **28**, 743 (1985).
- ⁴K. Sasaki, P. Hörling, T. Fall, J. H. Brzozowski, P. Brunsell, S. Hokin, E. Tennfors, J. Sallander, J. R. Drake, N. Inoue, J. Morikawa, Y. Ogawa, and Z. Yoshida, *Plasma Phys. Controlled Fusion* **39**, 333 (1997).
- ⁵J. M. McChesney, R. A. Stern, and P. M. Bellan, *Phys. Rev. Lett.* **59**, 1436 (1987).
- ⁶Z. Yoshida, *Nucl. Fusion* **31**, 386 (1991).
- ⁷K. Miyamoto, *Plasma Physics for Nuclear Fusion* (MIT, Cambridge, 1980), p. 625.
- ⁸N. Mattor, P. W. Terry, and S. C. Prager, *Comments Plasma Phys. Controlled Fusion* **15**, 65 (1992).
- ⁹A. G. Elfimov, R. M. O. Galvao, I. C. Nascimento, and G. Amarante-Segundo, *Plasma Phys. Controlled Fusion* **39**, 1551 (1997).
- ¹⁰R. Gatto and P. W. Terry, *Phys. Plasmas* **8**, 825 (2001).
- ¹¹S. Puri, *Phys. Fluids* **9**, 2043 (1966).
- ¹²D. J. D. Hartog and D. Craig, *Plasma Phys. Controlled Fusion* **42**, 47 (2000).
- ¹³S. R. Cranmer and A. A. van Ballegooijen, *Astrophys. J.* **594**, 573 (2003).
- ¹⁴S. R. Cranmer and A. A. van Ballegooijen, *Astrophys. J., Suppl. Ser.* **156**, 265 (2005).
- ¹⁵A. Hasegawa and L. Chen, *Phys. Fluids* **19**, 1924 (1976).
- ¹⁶R. M. Winglee, *Plasma Phys. Controlled Fusion* **26**, 511 (1984).
- ¹⁷S. Sridhar and P. Goldreich, *Astrophys. J.* **432**, 612 (1994).
- ¹⁸T. X. Zhang and B. Li, *Phys. Plasmas* **11**, 2172 (2004).
- ¹⁹R. Cross, *Introduction to Alfvén Waves* (Adam Hilger, Bristol, 1988).
- ²⁰A. Hasegawa and L. Chen, *Phys. Rev. Lett.* **35**, 370 (1975).
- ²¹E. D. Muller, *Math. Tables Aids Comput.* **10**, 208 (1956).
- ²²P. W. Terry, V. Tangri, J. S. Sarff, G. Fiksel, A. F. Almagri, Y. Ren, and S. C. Prager, *Fusion Energy Conference 2008 TH-C* (2008).
- ²³P. Goldreich and S. Sridhar, *Astrophys. J.* **483**, 763 (1995).
- ²⁴J. D. Huba, *NRL Plasma Formulary* (Wiley-VCH, Berlin, 2004).
- ²⁵A. R. Barakat and R. W. Schunk, *J. Phys. D* **14**, 421 (1981).
- ²⁶S. R. Cranmer, G. B. Field, and J. L. Kohl, *Astrophys. J.* **518**, 937 (1999).
- ²⁷N. F. Cramer, *The Physics of Alfvén Waves* (Wiley-VCH, New York, 2001), p. 312.
- ²⁸D. F. Diver, *A Plasma Formulary for Physics, Technology and Astrophysics* (Wiley-VCH, New York, 2001).
- ²⁹T. H. Stix, *Waves in Plasmas* (American Institute of Physics, New York, 1992).
- ³⁰J. V. Hollweg, *J. Geophys. Res.* **104**, 24793, DOI: 10.1029/1999JA900326 (1999).
- ³¹A. Lazaros, *Plasma Phys. Controlled Fusion* **31**, 1995 (1989).
- ³²G. P. M. Poppe and C. M. J. Wijers, *ACM Trans. Math. Softw.* **16**, 47 (1990).
- ³³A. Hasegawa and C. Uberoi, “Alfvén wave: DOE critical review series,” DOE/TIC-11197, Technical Information Center, U.S. Department of Energy, Springfield (1982).
- ³⁴V. A. Svidzinski, *Phys. Plasmas* **9**, 4392 (2002).
- ³⁵G. Rostagni, *Plasma Phys. Controlled Fusion* **36**, B203 (1994).